Physicochemical and Catalytic Properties of Copper Ethylenediamine Complex Encapsulated in Various Zeolites

R. Ganesan and B. Viswanathan*

Department of Chemistry, Indian Institute of Technology, Madras, Chennai 600036, India

Received: December 9, 2003; In Final Form: March 8, 2004

Bis(ethylenediamine)copper(II) $[Cu(NH_2CH_2CH_2NH_2)_2]^{2+}$(Cu-en) was encapsulated in NaY, KL, AlMCM-41, Naβ, and Na-ZSM-5. Characterization of the catalyst was done by IR, UV−vis, and electron paramagnetic resonance (EPR), whereas redox properties of neat and encapsulated Cu-en complexes were evaluated via cyclic voltammetry. The difference in UV−vis and EPR parameters between neat and intrazeolite complexes suggests that the metal complex does not have the same geometry as that in the neat complex but does undergo distortion inside the system. Peak broadening and different electrochemical responses are observed on encapsulation of the Cu-en complex in various zeolites, thus indicating that Cu-en complexes have altered values of redox potential in various positions of zeolite. Change of redox potential of Cu-en complex in zeolites is due to a change in the positions of the highest occupied molecular orbital (HOMO) and lowest unoccupied molecular orbital (LUMO) levels of the metal complexes. Density functional theory is used to calculate the position of the HOMO and LUMO levels of the metal complexes in zeolite cluster models. The HOMO and LUMO levels increase on encapsulation. When a substitution of the heteroatoms (B, Al, Ga) occurs, the HOMO and LUMO levels are stabilized, compared to those in pure silicious zeolites. An electric field acting inside the zeolite matrix is responsible for the change in the position of HOMO and LUMO levels of the metal complexes in various zeolites. Catalytic activity toward the oxidation of dimethyl sulfide by intrazeolite Cu-en complexes exhibits higher catalytic activity, compared to the neat complex.

1. Introduction

Enzymes catalyze various oxidation reactions in a regio- and stereo-controlled manner. They catalyze various electron-transfer reactions in a logical sequence, using appropriate redox centers.[1] Enzymes, which activate dioxygen to oxidize organic substrates into oxygenates, are classified into two groups, according to the mode of oxygen incorporation: dioxygenase and monooxygenase. Dioxygenase incorporates two O atoms, whereas monooxygenase transfers only one O atom. Iron, copper, and manganese are most frequently found in the active centers of oxygenases. The active centers in the enzymes consist of metal complexes with nitrogen- and oxygen-containing chelating ligands (porphyrin, chlorin, corrin). The ligands found in the biological systems prefer a planar or near-planar arrangement around a metal center. Assuming a total coordination number of 6 in an approximately octahedral arrangement, this planar arrangement leaves two axial coordination sites available at the metal center. For controlled stoichiometric or catalytic activation of substrates, there is indeed a need for two such open-coordination sites: one for the actual binding of the substrate and another for the regulation of catalytic activity. To mimic the biological systems, many synthetic complexes (metal porphyrins, metal phthalocyanins, and metal salen) that have the same active sites as in the biological systems are prepared. They catalyze various oxidation reactions, as in biological systems, but they lose their catalytic activity in one cycle itself, because of irreversible dimerization and irreversible oxidation of the ligands.[2,3] Living systems have found a way to frustrate irreversible dimerization and destruction of ligands by encapsulating active sites in a protein mantle (Figure 1). These protein mantles impose stearic constraints around a molecule for attack by other molecules. The stearic constraints around a metal complex induce tetragonal distortion of the octahedral symmetry or distorts from square planarity. This distortion causes characteristic splitting of the d-orbitals of coordinated transition-metal centers and leads to altered redox potentials of the metal complex in various protein mantles[4] (Figure 2). To increase the catalytic activity and stability of synthetic complexes, these complexes are encapsulated in various porous media and polymer matrixes. Among the porous media, zeolites are unique in the sense that the pore dimensions are not only uniform but also multidimensional in nature.[5] The complexes are stabilized inside the zeolite because of two factors. In the appropriate

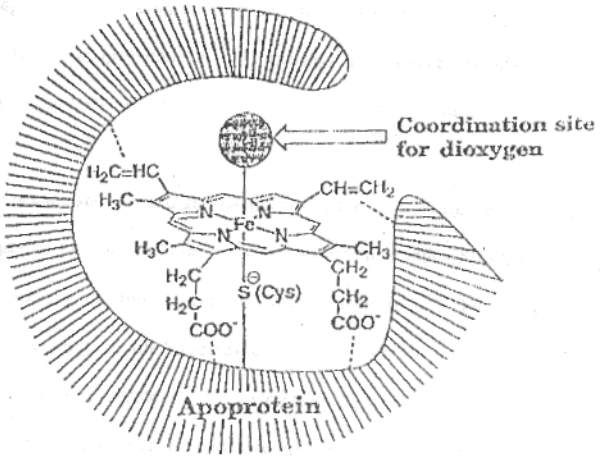

Figure 1. Active structure for cytochrome-P450.

* Author to whom correspondence should be addressed. Telephone: 91-44-22578250. FAX: 91-44-22578241. E-mail address: bvnathan@iitm.ac.in.

10.1021/jp037765o CCC: $27.50
Published on Web 04/29/2004

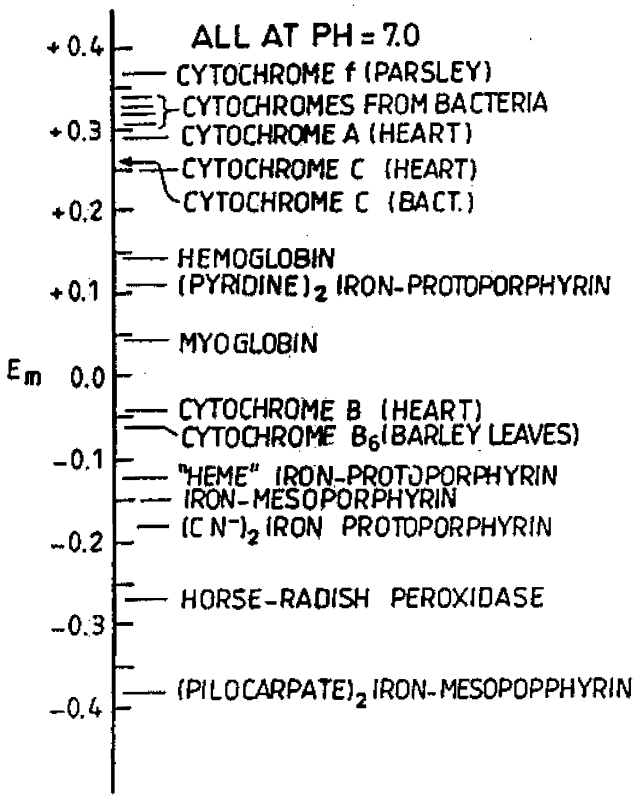

Figure 2. Redox potentials of various cytochromes. (Reproduced from ref 1.)

zeolite host, the molecule is free to move within the cavities of the zeolite but is prevented from leaching by restrictive pore openings (similar to a ship in a bottle).[6,7]

The interaction of certain functional groups of the complexes with some species on the walls of the zeolites can bind the metal complexes to the zeolites (host−guest interaction). This will prevent irreversible dimerization and destruction of the ligands. Metal complexes encapsulated in zeolites can mimic metalloenzymes and can therefore be called zeozymes.[8−10]

Copper is one of the metals most frequently found in biological systems. Many reports are available in the literature, which involve electron paramagnetic resonance (EPR) spectra of tetraamine copper complexes and tetrapyridine copper complexes in various zeolites (NaA, NaX, NaY, NaZSM-5, MCM-41, KL, mordenite).[11] Metal complexes present in the biological systems contain multidentate ligands. Encapsulation of copper complexes, which contain multidentate ligands in zeolite media, may mimic the biological systems that involve metal complexes encapsulated in a protein mantle. Peigneur et al. reported the encapsulation of copper ethylenediamine complexes in NaX and NaY zeolite media.[12] Bohlmann and Michel reported the encapsulation of a copper ethylenediamine complex in NaY, ZSM-5, and MCM-41.[13] Most of the reports on the encapsulation of metal complexes in zeolites involve the characterization of metal complexes by EPR and UV−vis spectroscopy. Only few reports have addressed the redox potential of metal complexes by cyclic voltammetry.[14−18] The reason for the alteration of metal complexes in a zeolite matrix is not clear in the literature. Selectivity is induced in biological systems by virtue of alteration of redox potential of metal complexes in various protein mantles. Similar type of systems can be generated by encapsulation of the same metal complexes in various zeolite matrixes. Keeping this in mind, an encapsulation of the copper ethylenediamine complex was performed in NaY, KL, Naβ, AlMCM-41, and NaZSM-5. The redox potentials of metal complexes were studied by cyclic voltammetry, and alteration of redox potential of metal complexes was rationalized based on the physical properties of zeolites.

2. Experimental Section

2.1. Materials. The chemicals used for the synthesis of copper ethylenediamine were copper nitrate (analytical grade (AR), E-Merck) and ethylenediamine (AR, CDH), as the sources of copper and ligand, respectively. NaY (Si/Al = 3) and KL (Si/Al = 3) zeolites were obtained from Ranbaxy Chemicals. Naβ (Si/Al = 30) and NaZSM-5 (Si/Al = 100) zeolites were obtained from Sud-Chemie. Dimethyl sulfide (DMS) was obtained from Fluka.

2.2. Preparation of the Copper Ethylenediamine Complex, ($Cu(NH_2CH_2CH_2NH_2)_2(NO_3)_2$ (Cu-en). To prepare the copper ethylenediamine complex, ($Cu(NH_2CH_2CH_2NH_2)_2(NO_3)_2$ (Cu-en),[19] 1 g of copper nitrate was dissolved in 25 mL of water and excess ethylenediamine was added to the solution (five times more than the stoichiometric amount). The resulting solution was boiled. Violet crystals, which separated out during the boiling, were filtered and washed with ethanol and diethyl ether. The resulting solid was dried at room temperature.

2.3. Preparation of Copper-Exchanged Zeolites. One gram of the respective zeolites was suspended in 100 mL of 0.1 M aqueous solution of copper nitrate and stirred for 24 h. The solution then was filtered and washed with excess water to remove any nitrate ions. The resulting solid was dried at room temperature.

2.4. Encapsulation of Copper Ethylenediamine Complexes in Various Zeolites. Copper-exchanged zeolites were calcined at 473 K. Approximately 1 g of dried copper-exchanged zeolites were suspended in 25 mL of ethylenediamine in a sealed round-bottom flask and stirred for 24 h. The resulting violet-colored materials were filtered, washed with excess water, and dried at room temperature.

2.5. Characterization. The copper content was estimated using Vogel's method.[19] The XRD patterns of all zeolites before and after encapsulation were recorded with a Philips automated powder diffractometer (Philips generator, Holland model PW1140) that was connected to an online recorder and a dot-matrix printer. The diffraction pattern was recorded using nickel-filtered Cu Kα radiation at a scanning rate of 3°/min and a chart speed of 3 mm per degree. IR studies in the range of 4000−400 cm^{-1} for neat zeolite-encapsulated metal complexes were recorded on a Shimadzu photometer. The samples were mixed well with KBr in 1:100 ratios and then pelletized. UV−vis spectra were recorded with a Lambda 17 spectrometer. For the neat complex, the spectra were recorded in water using a 1-cm quartz cell, whereas, for the encapsulated system, the spectra were recorded in Nujol mode at room temperature. The sample was diluted with Nujol oil and ground well in a mortar. The resulting paste was then soaked on a Whatmann No. 41 filter paper and was introduced into the spectrometer. Prior to that, background correction was done with Nujol-soaked filter paper. Electron spin resonance (ESR) spectra of neat complexes were recorded in appropriate solvents with a Varian E-112 spectrometer at liquid nitrogen temperature (77 K). For encapsulated systems, the spectra were obtained for the solid state by taking 50 mg of the sample in a quartz tube. The cyclic voltammograms of neat and encapsulated complexes were recorded on a Wenking potentioscan (model POS73) with a digital 2000 X−Y recorder, and 0.1 M phosphate buffer was used as the supporting electrolyte. The working electrode was prepared by taking a 1:1 weight ratio of neat or encapsulated metal complexes and

TABLE 1: Elemental Analyses for Neat and Zeolite-Encapsulated Cu-en Complexes

catalyst	Cu(II) content (wt %)	Cu-en concentration (mol/g)
Cu-en	20.8 (20.7)	
Cu-en-NaY	6.8	2.2×10^{-4}
Cu-en-KL	3.0	9.8×10^{-5}
Cu-en-Naβ	3.8	1.2×10^{-4}
Cu-en-AlMCM-41	2.6	8.4×10^{-5}
Cu-en-Na-ZSM-5	12.6	8.4×10^{-5}

Vulcan XC-72 carbon and dispersed in 1 mL of water. This suspension was ultrasonicated for 15 min. Ten microliters of this dispersion was coated on glassy carbon and 5 μL of 5% Nafion (as binder, from Aldrich) was added on these coatings and dried. This glassy carbon was used as the working electrode. Platinum foil was used as a counter electrode, and Ag/AgCl/KCl (saturated) was used as a reference electrode. The cyclic voltammogram of the neat complex was taken in solution mode, using 0.01 M of the metal complex in a phosphate buffer. Glassy carbon was used as a working electrode. Cyclic voltammograms for all the catalysts were taken in 50 mL of 0.1 M phosphate buffer (pH = 7).

2.6. Theoretical Methods. In the present investigations, the density functional theory (DFT) calculations were performed using the Gaussian 98 program. All DFT calculations were done by Becke three-parameter hybrid functions with the LYP correlation function (B3LYP) and an effective core potential basis set (LanL2DZ). Clusters of 10-membered-ring ($Si_{10}O_{10}H_{20}$) (D_{10h} symmetry, the model for ZSM-5) and 12-membered-ring ($Si_{12}O_{12}H_{24}$) (D_{12h} symmetry, the model for Fau) systems with 40 and 48 atoms, respectively, were used for the simulations, where the residual valence of the Si atoms were saturated with H atoms. The optimization of geometry was obtained using a universal force field approach (UFF1.02). In a typical calculation method, the metal complex was placed at the center of 10-membered-ring (Si_{10}) and 12-membered-ring (Si_{12}) systems and the geometry was optimized using a universal force-field approach. Cerius2 software was used for the force field calculations. Using force-field optimized parameters, DFT calculations were conducted at the B3LYP/LanL2DZ level. A similar approach has been attempted by Corma et al. for studying the interaction of alkenes in various zeolite cluster models.[20] A similar procedure was used to obtain force-field optimized geometries with different heteroatom (B, Al, Ga) substituted clusters.

2.7. Catalytic Activity. Liquid-phase oxidation of DMS was conducted in a glass reactor (double-necked round-bottom flask, with a capacity of 50 mL). The reactor was equipped with a reflux condenser. In a typical experiment, 100 mg of the desired catalysts was dispersed in 5 mL of water and a mixture of DMS and 30% hydrogen peroxide (H_2O_2) (1:1 molar ratio) were added and stirred for 24 h. At the end of the reaction, the reaction mixture was centrifuged and the products were analyzed in a gas chromatograph (Nucon) that was equipped with an OV 17 column.

3. Results and Discussion

3.1. Elemental Analysis. The metal content determined agrees well with the theoretically calculated value. It indicates that copper has 1:2 coordination (Table 1). There is no water of hydration present in the neat complex, which is also confirmed by thermogravimetric analysis (TGA), which shows that no weight loss is observed at ~100−120 °C. NaY zeolite has a greater metal content, because it has a greater amount of exchangeable cations.

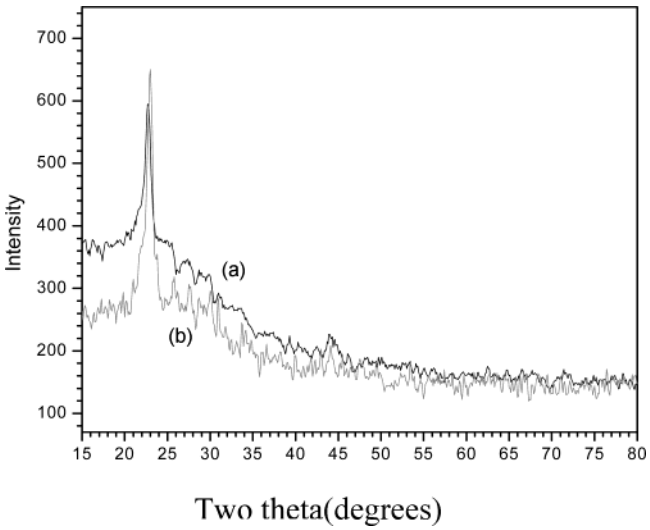

Figure 3. X-ray diffraction (XRD) pattern of (a) Naβ and (b) Cu-en-Naβ.

TABLE 2: C−H_{def} Bands of Cu-en in Neat and Zeolite-Encapsulated Complexes

catalyst	$\nu_{CH_{def}}$
Cu-en	1384
Cu-en-NaY	1355
Cu-en-KL	1355
Cu-en-Naβ	1354

3.2. X-ray Diffraction Studies. X-ray diffractometry (XRD) was recorded before and after encapsulation of the metal complexes. Figure 3a and b show the XRD pattern for Naβ zeolite before and after encapsulation of the copper ethylenediamine complex. The crystallinity of zeolite was maintained before and after encapsulation of the metal complexes. Similar trend is observed for other zeolites.

3.3. Infrared Spectroscopy. The concentration of metal complexes present in the zeolite is low. The observed bands, which correspond to metal complexes, are very weak. The lattice vibrations of the zeolite framework are observed in the range of 400−1300 cm^{-1}.

Most of the ligands used give a characteristic band in the region of 1200−1600 cm^{-1} (Table 2). The bands observed (1583.2 (NH_2 def), 1384.2 (CH_2 def), 1277.1 (NH_2 def)) for the neat copper ethylenediamine complex (Figure 4a) agree with the values reported in the literature.[21] On encapsulation of the metal complexes in various zeolites, weak bands were observed in the region of 1600−1200 cm^{-1} (Figure 4b−d). It indicates the formation of metal complexes. The CH_2 (def) band is shifted toward lower wavenumber (Table 2) on encapsulation in various zeolites. This indicates the interaction of the metal complex in various zeolites.[22−27]

3.4. UV−Vis Spectroscopy. The copper ethylenediamine complex has D_{2h} symmetry. The energy-level diagrams for ligand fields with D_{2h} symmetry would predict four transitions, whereas that of D_{4h} symmetry would require three transitions. The splitting of the ^2E_g level in D_{2h} symmetry is small in going from D_{4h} symmetry. The spectrum is poorly resolved; therefore, D_{4h} symmetry was assumed in all the systems. In D_{4h} symmetry, the $^2B_{2g}$ level will always lie below the ^2E_g level. The spectrum of copper ethylenediamine in water shows a broad band at 18 315 cm^{-1}. It is difficult to assign the observed values to any one of the transitions. The broad band consists of all three/four transitions. The transition from $^2B_{1g} \rightarrow {}^2E_g$ is highly intense.[12] Peigneuer et al. assumed that the band observed at 18 315 cm^{-1}

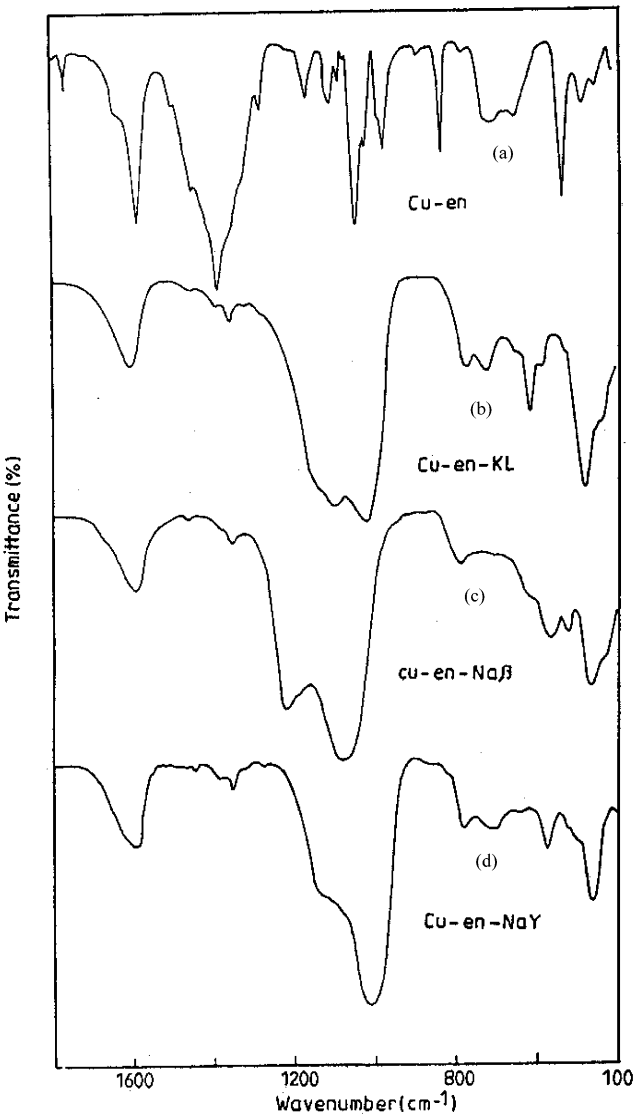

Figure 4. IR spectra of (a) Cu-en, (b) Cu-en-KL, (c) Cu-en-Naβ, and (d) Cu-en-NaY.

corresponds to the $^2B_{1g} \rightarrow {}^2E_g$ (ΔE_{xz}) transition (Figure 5a).[12] Lewis et al. assumed that the same band corresponds to the $^2B_{1g} \rightarrow {}^2B_{2g}$ (ΔE_{xy}) transition.[28] Wasson and Trapp assumed, for copper complexes, that the maximum in the band corresponds to the $^2B_{1g} \rightarrow {}^2B_{2g}$ transition and the wavelength of the band at one-half of the maximum corresponds to the $^2B_{1g} \rightarrow {}^2E_g$ transtition.[29] Because the $^2B_{1g} \rightarrow {}^2E_g$ transition can be estimated from the spin Hamiltonian parameters, which comes to be 28 600 cm^{-1}, the band at 28 600 cm^{-1} could be masked by a strong ultraviolet absorption band. Gersmann and Swalen assigned the peak maximum observed in the range of 18 000−21 000 cm^{-1} to the $^2B_{1g} \rightarrow {}^2B_{2g}$ transition and the value observed in the range of 23 100−31 000 cm^{-1} corresponds to the $^2B_{1g} \rightarrow {}^2E_g$ transition for various copper complexes.[30] Using optical absorption data from several sources for copper complexes, it is assumed that the band observed at 18 315 cm^{-1} corresponds to the $^2B_{1g} \rightarrow {}^2B_{2g}$ transition (Table 3). This transition is blue-shifted on encapsulation in NaY zeolite (Figure 5b) (916 cm^{-1}) but is red-shifted in Naβ zeolite (Figure 5c) (458 cm^{-1}), Na-ZSM-5 zeolite (Figure 5f) (771 cm^{-1}), and AlMCM-41 (Figure 5e) (521 cm^{-1}). Similar features were observed by Jacob et al. when copper phthalocyanine complexes were encapsulated in NaX and NaY zeolites.[31] The $\pi \rightarrow \pi^*$ transition of the phthalocyanine ligand is red-shifted on encapsulation of copper phthalocyanine in NaY zeolite, but it is blue-shifted in NaX zeolite. Chavan et al. observed a blue shift when a dimeric copper acetate complex was encapsulated in NaY zeolite, but it was red-shifted when a dimeric copper chloro acetate complex was encapsulated in a NaY zeolite matrix.[32] For most of the transtition-metal complexes, the general feature observed for distortion from square planar geometry is a red shift and intensity enhancement of the d−d bands.[33−38] The shift in peak maximum (Table 3) suggests that the molecule is not maintaining the same electronic structure as that in the neat complex but may undergo distortion inside a constrained zeolite environment.

3.5 EPR Spectroscopy. 3.5.1. EPR of Copper Ethylenediamine Complex. The free Cu ion has a ^2D term symbol. When the free Cu ion is placed in a complex, the ^2D term is split into several states. The energy levels are shifted from the free ion position. The splitting of energy of the d-orbital is related to the chemical properties of the complexes.

The symmetry of the copper ethylenediamine complex is assumed to be square planar (D_{2h}). The gyromagnetic ratios for these complexes have the values

$$g_{\parallel} = 2 + \frac{8\lambda}{E_0 - E_2} \tag{3.1a}$$

and

$$g_{\perp} = 2 + \frac{2\lambda}{E_0 - E_3} \tag{3.1b}$$

where E_2 is the B_{2g} state (d_{xy}), E_3 the E_g state (d_{yz} and d_{xz}), and λ the spin−orbit coupling constant (828 cm^{-1} for Cu^{2+}). The aforementioned equation does not take ligand field transitions into consideration. Using group theory, the proper linear combinations of ligand orbitals can be combined with the Cu d-orbitals to form the following antibonding wave functions:[39,40]

$$\psi_{B_{1g}} = \alpha d_x 2 - {}_y 2 - \frac{1}{2}\alpha'[-\sigma_x^{(1)} + \sigma_y^{(2)} + \sigma_z^{(3)} - \sigma_y^{(4)}] \tag{3.2}$$

$$\psi_{B_{2g}} = \beta d_{xy} - \frac{1}{2}(1-\beta^2)^{1/2}[p_y^{(1)} + p_x^{(2)} - p_y^{(3)} - p_x^{(4)}] \tag{3.3}$$

$$\psi_{A_{1g}} = \gamma d_{3z} 2 - {}_r 2 - \frac{1}{2}(1-\gamma^2)^{1/2}[\sigma_x^{(1)} + \sigma_y^{(2)} - \sigma_z^{(3)} - \sigma_y^{(4)}] \tag{3.4}$$

$$\psi_{E_g} = \delta d_{xz} - (1-\delta^2)^{1/2}\left(\frac{p_z^{(1)} - p_z^{(3)}}{\sqrt{2}}\right) \tag{3.5}$$

$$\psi_{E_g} = \delta d_{yz} - (1-\delta^2)^{1/2}\left(\frac{p_z^{(2)} - p_z^{(4)}}{\sqrt{2}}\right) \tag{3.6}$$

Overlap is included only for the $^{\psi}B_{1g}$ state, where α and α' are related:

$$\alpha^2 + \alpha'^2 - 2\alpha\alpha' S \tag{3.7}$$

Here, S is the overlap integral. For nitrogen-containing ligands, the value of S is 0.093. The B_{1g} and A_{1g} states account for the σ bonding to the copper (α and α'). The B_{2g} state represents the in-plane π-bonding (β). The E_g term represents the out-of-plane π-bonding (γ, δ). The smaller the value of α, α', β, γ, and δ, the more covalent the character. When an unpaired electron is interacting with a magnetic field,

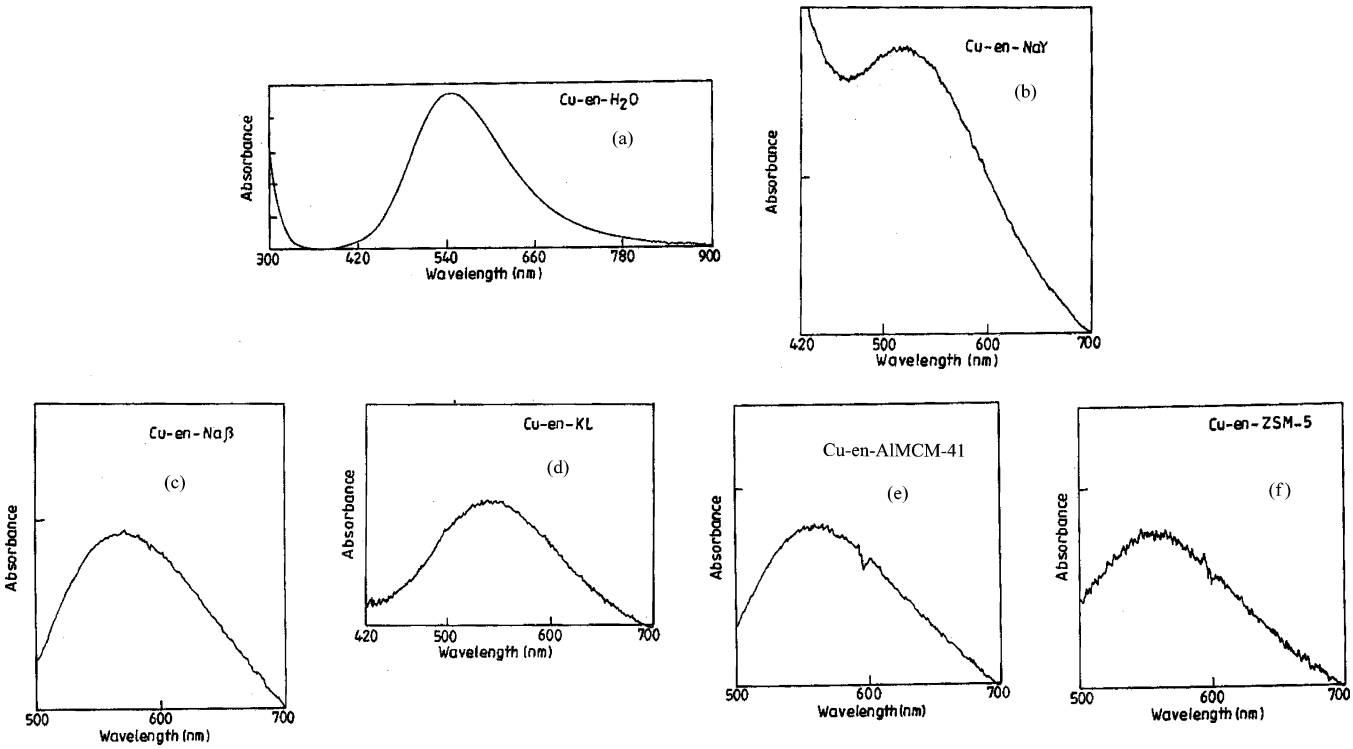

Figure 5. UV−vis spectra of (a) Cu-en-H_2O, (b) Cu-en-NaY, (c) Cu-en-Naβ, (d) Cu-en-KL, (e) Cu-en-AlMCM-41, and (f) Cu-en-NaZSM-5.

TABLE 3: Bonding Parameters and UV−Vis Spectral Parameters for Neat and Zeolite-Encapsulated Cu-en Complexes

catalyst	α^2	α'^2	β^2	ΔE_{xy}	λ_{eff} (cm^{-1})
Cu-en-H_2O	0.83	0.24	0.74	18315	473
Cu-en-NaY	0.83	0.24	0.77	19231	492
Cu-en-KL	0.85	0.21	0.69	18315	455
Cu-en-Naβ	0.82	0.25	0.74	17857	464
Cu-en-NaZSM-5	0.83	0.24	0.70	17794	449
Cu-en-AlMCM-41	0.82	0.25	0.70	17544	440
$Cu(H_2O)_6^{2+}$	0.90	0.16			
Cu-NaY	0.95	0.10			
Cu-KL	0.89	0.17			
Cu-Naβ	0.91	0.15			
Cu-NaZSM-5	0.91	0.15			
Cu-AlMCM-41	0.94	0.11			

the spin Hamiltonian is given by

$$\mathcal{H} = g_{\parallel}\beta H_z S_z + g_{\perp}\beta(H_x S_x + H_y S_y) + A_{\parallel} S_z I_z + A_{\perp}(S_x I_x + S_y I_y) \quad (3.8)$$

When the wave function for the B_{1g} is applied to the aforementioned Hamiltonian, the following magnetic parameters can be obtained:

$$g_{\parallel} = 2.0023 - \left(\frac{8\lambda}{\Delta E_{xy}}\right)[\alpha^2\beta^2 - f(\beta)] \quad (3.9)$$

where $f(\beta) = \alpha\alpha'\beta^2 S + \alpha\alpha'\beta(1-\beta^2)^{1/2}T(n)/2$,

$$g_{\perp} = 2.0023 - \left(\frac{2\lambda}{\Delta E_{xx}}\right)[\alpha^2\delta^2 - f(\delta)] \quad (3.10)$$

where $f(\delta) = \alpha\alpha'\delta^2 S + \alpha\alpha'\delta\,(1-\delta^2)^{1/2}T(n)/\sqrt{2}$, and

$$A_{\parallel} = P\left\{\alpha^2\left(\frac{4}{7} + k\right) - 2\lambda\alpha^2\left[\frac{4\beta^2}{\Delta E_{xy}} + \left(\frac{3}{7}\right)\frac{\delta^2}{\Delta E_{xz}}\right]\right\} \quad (3.11)$$

where $P = 2\gamma_{Cu}\beta_0\beta_N\langle \times e1(d_x2 - {}_y2)(1/r^3)(d_x2 - {}_y2)\rangle = 0.036$ cm^{-1}, γ_{Cu} is the magnetic moment of copper (Cu^{63} or Cu^{65}), β_0 is the Bohr magneton, and β_N is the nuclear magneton. The constant k corrects for the Fermi contact term of excited configurations of Cu ($3s3d^{10}$ and $3d^84s$). The constant $T(n)$ is an integral over the ligand functions and results from the calculation of the matrix elements of the Hamiltonian with the wave functions. Based on these equations, α can be approximately evaluated using the following equation:[30]

$$\alpha^2 = \frac{A_{\parallel}}{P} + (g_{\parallel} - 2) + \left(\frac{3}{7}\right)(g_{\perp} - 2) + 0.04 \quad (3.12)$$

Here, 0.04 approximates the various integrals by an average value.

The α values (the metal d-orbital coefficients for the b_{1g} molecular orbital representing in-plane σ-bonding) were calculated from eq 3.12, whereas the value of α' (the metal d-orbital coefficients for the b_{1g} molecular orbital representing in-plane σ-bonding) was calculated from eq 3.7. The value of β (the metal d-orbital coefficients for the b_{2g} molecular orbital representing in-plane π-bonding) was calculated from eq 3.9, using the ΔE_{xy} value from UV−vis spectroscopy.

The $g_{\parallel}$ and $g_{\perp}$ values can be correlated to effective spin−orbit coupling by the following equations:[12]

$$g_{\parallel} = 2.0023 - \left(\frac{8\lambda_{eff}}{\Delta E_{xy}}\right) \quad (3.13)$$

$$g_{\perp} = 2.0023 - \left(\frac{2\lambda_{eff}}{\Delta E_{xz}}\right) \quad (3.14)$$

The ΔE_{xy} value can be calculated from UV−vis spectroscopy. Using eq 3.13, the effective spin−orbit coupling constant value was calculated.

3.5.2. EPR Spectra of Cu-en. EPR spectra of the polycrystalline Cu-en sample show two g values ($g_1 = 2.24$ and $g_2 =$

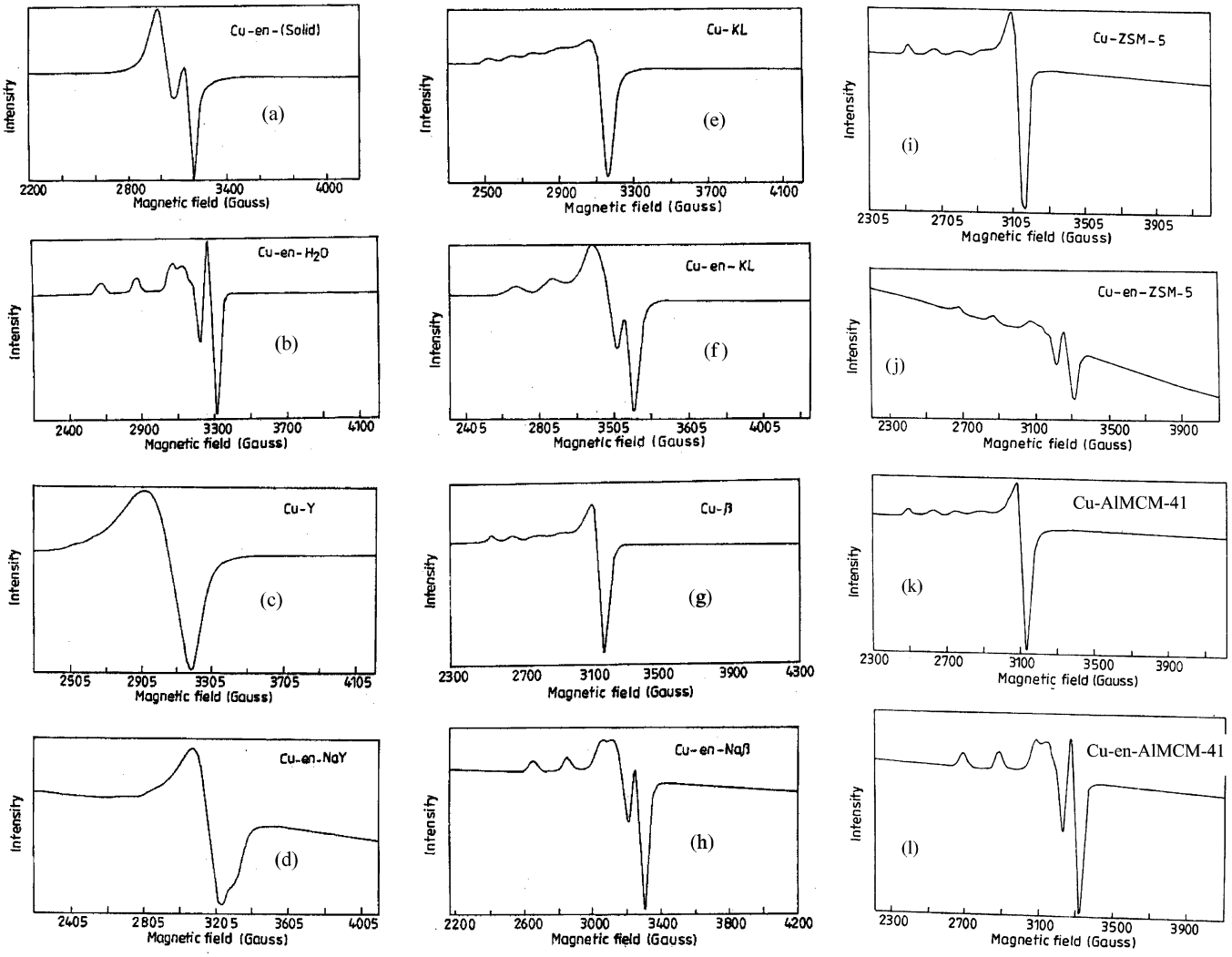

Figure 6. EPR spectra of (a) Cu-en (solid), (b) Cu-en in H_2O, (c) Cu-Y, (d) Cu-en-NaY, (e) Cu-KL, (f) Cu-en-KL, (g) Cu-β, (h) Cu-en-Naβ, (i) Cu-ZSM-5, (j) Cu-en-ZSM-5, (k) Cu-AlMCM-41, and (l) Cu-en-AlMCM-41.

TABLE 4: EPR Spectral Parameters for Neat and Zeolite-Encapsulated Cu-en Complexes

catalyst	$g_{\|\|}$	$g_\perp$	$A_{\|\|}$(gauss)	$A_{\|\|}$ ($\times 10^{-4}$ cm^{-1})
Cu-en-H_2O	2.209	2.047	198	201
Cu-en-NaY	2.207	2.051	200	203
Cu-en-KL	2.201	2.067	205	208
Cu-en-Naβ	2.210	2.064	195	198
Cu-en-NaZSM-5	2.204	2.056	200	203
Cu-en-AlMCM-41	2.203	2.058	195	198
$Cu(H_2O)_6^{2+}$	2.400	2.099	137	151
Cu-NaY	2.397	2.197	140	154
Cu-KL	2.427	2.099	125	140
Cu-Naβ	2.409	2.097	135	150
Cu-NaZSM-5	2.399	2.097	140	154
Cu-AlMCM-41	2.443	2.113	130	146

2.071) that are characteristic of a normal tetragonal environment (Figure 6a). Hyperfine coupling is not resolved in polycrystalline samples, because of the higher exchange coupling between Cu centers.[41] The Cu-en sample was dissolved in a 50% water and glycerol mixture and the EPR spectrum was recorded. The EPR spectrum is characteristic of ions with an axially symmetric g-tensor. In the parallel direction, most of the hyperfine components are resolved; however, in the perpendicular direction, the hyperfine splitting is small and the components are not resolved (Figure 6b). It has been observed that, for all copper systems, $g_{\|} > g_\perp > 2.0023$, indicating that the unpaired electron is present in the d_x2-_y2 orbital, which is characteristic of Cu ions that undergo tetragonal elongation. The parameters for the Cu-en complex (Table 4) in a 50% water and glycerol mixture obtained from this study ($g_{\|} = 2.209$, $g_\perp = 2.047$, and $A_{\|} = 201$ cm^{-1}) are similar to the values previously reported by Lewis et al.[28] The bonding parameter (see Table 3) shows that the molecular orbital coefficients vary in the order $\alpha > \beta$, suggesting that the in-plane π-bonding is more covalent than the in-plane σ-bonding. The spin−orbit coupling constant for the free Cu ion is -828 cm^{-1}. It decreases when it is coordinated to ethylenediamine. The spin−orbit coupling is related to ϵ by the equation

$$\lambda = \pm\frac{\epsilon}{2S}$$

where ϵ is a measure of the energy of the interaction between the spin and the orbital angular moment of a single electron of the configuration. This is proportional to effective nuclear charge and inversely proportional to average distance of the electron from the nucleus. S is the spin multiplicity of an atom.

Delocalization of the electrons, as well as shielding of the nucleus by the ligand electrons, can decrease the value of λ. The decrease of spin−orbit coupling on coordination of the Cu ion with the ethylenediamine ligand indicates the enhanced covalent bonding between the Cu ion and the ethylenediamine ligand.

3.5.3. EPR Spectra of Cu-Y and Cu-en-NaY. Y zeolite consists of a three-dimensional (3-D) network of AlO_4 and SiO_4 tetrahedra with a Si/Al ratio of ~1.2. These tetrahedral units are linked to each other by sharing all of the oxygens to form truncated octahedra called sodalite or β-cages. The sodalite cages are interconnected through a double six-membered ring (hexagonal prism) to form a larger cage called super cage or α-cage. The free diameter of the α-cage and β-cages are 0.74 and 0.22 nm, respectively. Because of the excess charge present on the AlO_2 units, charge-compensating cations are present to neutralize the negative charge. Various cation sites are present in the Y zeolite. The SU and SV sites are located at the centers of the β- and α-cages, respectively. The SI site is located at the center of the hexagonal prism. SI′ is a site displaced into the β-cage from the hexagonal prism. The SII site is located at the center of the hexagonal window between the β- and α-cages. SII′ and SII* correspond to the displacement from site SII into the β- and α-cages, respectively. The EPR spectra of hydrated copper-exchanged Y zeolites are shown in Figure 6c. The EPR spectrum exhibits hyperfine features that are characteristic of the Cu nucleus with $I = {}^3/_2$. The hyperfine features are poorly resolved in Y zeolites, compared to those in other zeolites. This may be due to the higher concentration of Cu ions present in the cages. The set of parameters (Table 4) with values of $g_{\|} = 2.397$ and $A_{\|} = 140$ G is assigned to the hexa aqua copper complex ($Cu(H_2O)_6^{2+}$) present in the zeolite cages.[11,42,43] For comparison, the EPR spectrum of $Cu(H_2O)_6^{2+}$ in a glycerin−water mixture gives a set of parameters with the values of $g_{\|} = 2.400$ and $A_{\|} = 137$ G. The EPR spectrum of copper-exchanged zeolites is taken without preactivation. Hermann and Flentge reported that, without preactivation and an equilibration time of 16 h of copper salts with zeolites during preparation, all $Cu(H_2O)_6^{2+}$ units are preferentially held in the super cages in copper-exchanged Y zeolite.[42] On activation, Cu ions migrated to the sodalite cages. The parameters observed in this study for Cu ions correspond to hexa aqua copper ions present in the super cages.

The copper-exchanged zeolite is calcined at 200 °C in air and cooled to room temperature. Ethylenediamine is added to the copper-exchanged zeolite and stirred for 24 h. It is washed with excess water and dried at room temperature. The EPR spectrum recorded at 77 K after adsorption of ethylenediamine is shown in Figure 6d. Several changes were observed after the adsorption of ethylenediamine on the copper-exchanged zeolites. The g value decreases and the $A_{\|}$ value increases on adsorption of ethylenediamine on copper-exchanged zeolites (see Table 4). It is known that, when the symmetry of the ligand field of the copper complex changes from the octahedral via square pyramidal coordination to a planar environment, the $g_{\|}$ value decreases and the $A_{\|}$ value increases.[44] The $g_{\|}$ and $A_{\|}$ values suggest the formation of a copper ethylenediamine complex with 1:2 coordination. Bohlmann and Michel reported similar EPR parameters for a copper ethylenediamine complex in NaY zeolite.[13] The EPR parameters reported in this work and reported by Bohlmann and Michel[13] are different than the values reported by Peigneur et al.[12] The EPR parameters and UV−vis bands are sensitive to the mode of preparation of the metal complexes, loading, pretreatment procedure, and Si/Al ratio.[45,46] The hyperfine coupling constant value is characteristic of the coordination of copper. Monoethylenediamine copper(II) ($Cu(en)^{2+}$) has a hyperfine coupling constant value of 172 G and that for bis(ethylenediamine) copper(II) is 199 G.[22] The g and A values observed on encapsulation in zeolites are consistent with the Cu-en in 1:2 coordination ($Cu(en)_2^{2+}$). The molecular dimension of Cu-en is ~5 Å. This molecule can be located both in sodalite cages and super cages. The EPR spectrum is poorly resolved; therefore, it is difficult to differentiate the copper complexes present in the sodalite cages and super cages. The bonding parameters suggest that the in-plane σ-bonding (α = 0.95 for Cu-Y and 0.83 for Cu-en-NaY) becomes more covalent on adsorption of ethylenediamine on copper-exchanged zeolite (see Table 3). This clearly shows enhanced covalent bonding between the ethylenediamine and the copper when copper ethylenediamine complex is formed in zeolite cages. The molecular orbital coefficient for in-plane π-bonding of copper ethylenediamine in NaY zeolite is higher, compared to that of the neat complex ($\beta = 0.74$ for Cu-en and 0.77 for Cu-en-NaY; see Table 3). This indicates that bonding is more ionic in Cu-en NaY than in neat copper ethylenediamine. Similarly, the effective spin−orbit coupling increases ($\lambda_{eff} = 473$ cm^{-1} for Cu-en and 493 cm^{-1} for Cu-en NaY) on encapsulation of the copper ethylenediamine complex in zeolite Y. The difference in molecular orbital coefficients and spin−orbit coupling constant suggests that the copper ethylenediamine molecule may undergo distortion inside the zeolite Y and any different behavior of the copper ethylenediamine complexes on encapsulation in NaY zeolite may be caused by a change in the wave function of the metal complexes.

3.5.4. Electron Paramagnetic Resonance of Cu-KL and Cu-en-KL Zeolites. Zeolite L is a synthetic aluminosilicate with a common Si/Al ratio of 3. The crystal structure of the zeolite is based on the ϵ-cages of the 18-tetrahedra unit found in cancrinite, which are formed by five six-membered rings and six four-membered rings. The ϵ-cages are linked through two almost-planar six-membered rings, forming hexagonal prisms with the planes of the six-membered rings normal to the ***c***-axis. Thus, zeolite L consists of a series of columns along the *c*-axis, where ϵ-cages and hexagonal prisms alternate. These columns are linked to each other, producing wide channels of 12-membered rings parallel to the ***c***-axis. These wide channels have free diameters of 0.71−0.78 nm. The largest internal diameter of the 12-membered rings is ~1.3 nm. The walls of the internal channels consist of eight- and four-membered rings. The main channels are connected to each other through nonplanar eight-membered rings. There are five types of cation sites located for Na^+ and K^+ ions in KL zeolites. Site A is located in the center of hexagonal prism. This site is comparable to an SI site in the middle of a hexagonal prism in zeolite X. The cation in site A forms distorted octahedral coordination with six framework oxygens, three above and three below the cation. Site B is the center of the ϵ-cage. Site C is located midway between the centers of two ϵ cages. Site D is located in the main channels. The cation in site D coordinates to four framework oxygens in the nonplanar eight-membered ring. Site E is located midway between two adjacent A sites.

The hydrated copper-exchanged KL zeolite at 77 K gives an asymmetric spectrum (see Table 4), with $g_{\|} = 2.427$, $g_{\perp} = 2.099$, and $A_{\|} = 125$ G (140 × 10^{-4} cm^{-1}) (Figure 6e). This value is consistent with the values reported in the literature ($g_{\|} = 2.412$, $g_{\perp} = 2.080$, and $A_{\|} = 123$ G (137 × 10^{-4} cm^{-1}).[47,48] This value corresponds to the hexa aqua copper complex ($Cu(H_2O)_6^{2+}$). Zeolite L has 12-membered-ring main channels whose diameter is ~0.75 nm. Among all the possible cation sites, 12-membered-ring main channels are the only possible locations for accommodation of $Cu(H_2O)_6^{2+}$ in zeolite L.

The adsorption of ethylenediamine on copper-exchanged KL zeolites produces new cupric species (Figure 6f) with ESR parameters $g_{\|} = 2.201$, $g_{\perp} = 2.087$, and $A_{\|} = 205$ G (208 ×

10^{-4} cm^{-1}) (see Table 4). The changes in the EPR spectrum on adsorption of ethylenediamine on copper-exchanged KL zeolites indicate the formation of copper ethylenediamine complex in the KL zeolites. The observed ESR parameters indicate that the Cu ion is in square planar environment and tetra-coordinated. The tetra-coordinated copper complex may be located in the main channel of the 12-membered ring.

The bonding parameters suggest that the in-plane σ-bonding ($\alpha = 0.95$ for Cu−KL and 0.83 for Cu-en-KL) (see Table 3) becomes more covalent on the adsorption of ethylenediamine on copper-exchanged KL zeolite. This clearly shows enhanced covalent bonding between ethylenediamine and copper on formation of the copper ethylenediamine complex in zeolite cages. The in-plane π-bonding of copper ethylenediamine in zeolite KL is more covalent in comparison with neat copper ethylenediamine complex ($\beta = 0.74$ for Cu-en and 0.69 for Cu-en-KL) (see Table 3). Similarly, effective spin−orbit coupling decreases ($\lambda_{eff} = 473$ cm^{-1} for Cu-en and 455 cm^{-1} for Cu-en KL) on encapsulation of the copper ethylenediamine complex in zeolite KL. The decrease in effective spin−orbit coupling constant and molecular orbital coefficients for in-plane π-bonding on encapsulation of the copper ethylenediamine complex in KL zeolite indicates the increase in covalency between the metal and the ligand. This may be due to distortion of the metal complex from square planarity inside the zeolite matrix.

3.5.5. EPR of Cu-β and Cu-en-β Zeolite. β-Zeolite belongs to the family of pentasil zeolites. There are three possible cation sites in β-zeolites. Site A is located in the center of six-membered rings, and sites B and C correspond to the cation position in two different five-membered rings. Along the [100] direction, there is a channel (12-membered ring) with an elliptical cross section of 6.6 Å × 6.7 Å (diameter). Another channel exists along the [001] direction. It is comprised of a 12-membered ring with an elliptical cross section of 5.6 Å × 5.6 Å (molecular diameter). The EPR spectrum of the hydrated copper-exchanged zeolites is shown in Figure 6g. The observed EPR spectrum indicates the presence of $Cu(H_2O)_6^{2+}$ inside the zeolite matrix (see Table 4). The $Cu(H_2O)_6^{2+}$ may be present in the main channel of the 12-membered ring.[49] After adsorption of the ethylenediamine ligand on copper-exchanged β-zeolite, the $g_{||}$ values decrease and the $A_{||}$ value increases (see Table 4). The $g_{||}$ and $A_{||}$ values suggest the presence of a tetra-coordinated copper complex in a square planar environment (see Figure 6h). The bonding parameters suggest that the in-plane σ-bonding ($\alpha = 0.91$ for Cu-β and 0.82 for Cu-en-β) becomes more covalent on adsorption (see Table 3) of ethylenediamine on the copper-exchanged β-zeolite. This clearly shows enhanced covalent bonding between the ethylenediamine and the copper on the formation of a copper ethylenediamine complex in zeolite cages. The effective spin−orbit coupling constant decreases (λ_{eff} = 473 cm^{-1} for Cu-en and 464 cm^{-1} for Cu-en-β) on encapsulation of a copper ethylenediamine complex in β-zeolite (see Table 3). The decrease in effective spin−orbit coupling constant may be due to distortion of the metal complex from square planarity inside the zeolite matrix.

3.5.6. EPR of Cu-ZSM-5 and Cu-en-ZSM-5 Zeolite. The structure of zeolite ZSM-5 consists mainly of five-membered rings (rings containing five tetrahedral units and five bridging O atoms) that are linked together to give a system of channels. Running parallel to the crystallographic [010] direction are straight channels with an elliptical cross section of 0.54 nm × 0.56 nm (diameter). Perpendicular to these channels run cross-linking zigzag elliptical channels with dimensions of 0.51 nm × 0.55 nm (diameter). Possible cation locations lie close to the walls of the channels adjacent to four rings, five rings, or six rings. There are also possible cation sites that are recessed from the main channel in side pockets. Finally, there are sites totally inaccessible to the main channels, which are located within the chains of the lattice structure, which lie parallel to the *z*-direction. As in the zeolites NaY, KL, and Naβ, there is no standard nomenclature for cation locations in ZSM-5.

The hydrated copper-exchanged Na-ZSM-5 zeolite at 77 K gives an asymmetric spectrum, with $g_{||} = 2.397$, $g_{\perp} = 2.097$, and $A_{||} = 140$ G (154×10^{-4} cm^{-1}) (see Table 4). This value is consistent with the values reported in the literature ($g_{||} = 2.389$, $g_{\perp} = 2.092$, and $A_{||} = 12$ G (147×10^{-4} cm^{-1})[44−46] (see Figure 6i). This value corresponds to the hexa aqua copper complex $Cu(H_2O)_6^{2+}$, which has a molecular dimension of 0.74 nm. The molecular dimension of $Cu(H_2O)_6^{2+}$ is very large to be accommodated in the elliptical channels. The molecule can be accommodated only at the intersection of two channels, where there is an increase in available space.

The adsorption of ethylenediamine changes the ESR parameters (Figure 6j). The ESR parameters indicate the square planar nature of the complex (see Table 4). This complex may be located in the intersection of two channels. The bonding parameters suggest that the in-plane σ-bonding ($\alpha = 0.91$ for Cu-ZSM-5 and 0.83 for Cu-en-ZSM-5) becomes more covalent on adsorption of ethylenediamine on copper-exchanged ZSM-5 zeolite (see Table 3). This clearly shows enhanced covalent bonding between ethylenediamine and copper when copper ethylenediamine complex is formed in zeolite cages. The in-plane π-bonding of copper ethylenediamine in ZSM-5 zeolite is more covalent in comparison with the neat copper ethylenediamine complex ($\beta = 0.74$ for Cu-en and 0.70 for Cu-en-ZSM-5) (see Table 3). Similarly effective spin−orbit coupling decreases (λ_{eff} = 473 cm^{-1} for Cu-en and 449 cm^{-1} for Cu-en-ZSM-5) on encapsulation of copper ethylenediamine complex in zeolite ZSM-5. The decrease in effective spin−orbit coupling constant and molecular orbital coefficients for in-plane π-bonding on encapsulation of the copper ethylenediamine complex in zeolite ZSM-5 indicates the increase in covalency between metal and ligand. This may be due to distortion of the metal complex from planarity inside the zeolite matrix.

3.5.7. Cu-AlMCM-41 and Cu-en-AlMCM-41. MCM-41 is member of the M41S type of mesoporous solids with uniform hexagonal pores. The diameters of the pores range from 20 Å to >100 Å. The EPR spectra (Figure 6k) of copper-exchanged AlMCM-41 show the presence of $Cu(H_2O)_6^{2+}$ (see Table 4), which is present in the main channels of AlMCM-41.[50]

On adsorption of ethylenediamine on copper-exchanged AlMCM-41, an EPR pattern that is characteristic of the copper ethylenediamine complex in 1:2 coordination can be observed (see Figure 6l). The bonding parameter indicates that in-plane π-bonding becomes more covalent after the adsorption of ethylenediamine on copper-exchanged AlMCM-41 (see Table 3). The difference in spin−orbit coupling constant and molecular orbital coefficients suggests that the complex molecule may undergo distortion inside the AlMCM-41.

3.6. Cyclic Voltammetry. Cyclic voltammetry provides information on the nature of intrazeolite complexes that may not be readily apparent from spectroscopic studies. The voltammogram of a neat complex in solution mode (0.1 M phosphate buffer) shows a couple of peaks with values of $E_{pc} = -238$ mV and $E_{pa} = -4$ mV (Table 5). This redox process, when associated with a cathodic peak, is the reduction of copper ethylenediamine to copper ($Cu(en)_2^{2+}$/Cu) and, when associated

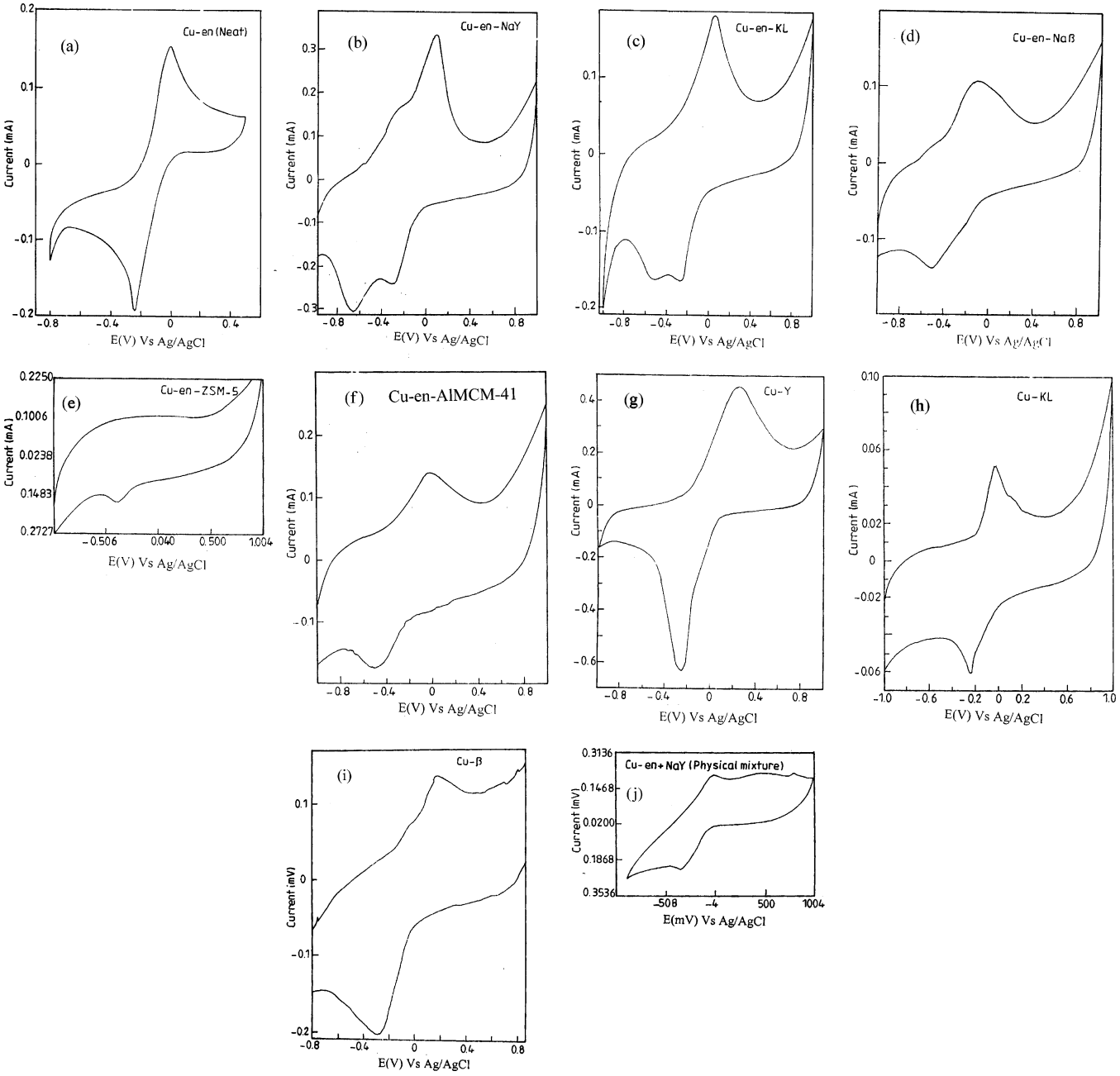

Figure 7. Cyclic voltammogram of (a) Cu-en (neat), (b) Cu-en-NaY, (c) Cu-en-KL, (d) Cu-en-Naβ, (e) Cu-en-ZSM-5, (f) Cu-en-AlMCM-41, (g) Cu-NaY, (h) Cu-KL, (i) Cu−Naβ, and (j) Cu-en + NaY (physical mixture).

TABLE 5: Cyclic Voltammetric Data for Neat and Zeolite-Encapsulated Cu-en Complexes

catalyst	E_{pc} (mV)	E_{pa} (mV)
Cu-en	−238	−4
Cu-en-NaY	−672 −308	−96
Cu-en-KL	−268 −504	−64
Cu-en-Naβ	−516	−96
Cu-en-AlMCM-41	−504	−20
Cu-en-NaZSM-5	−397	+86
Cu-NaY	−252	276
Cu-KL	−240	−36
Cu-Naβ	−268	172

with an anodic peak, is the oxidation of deposited copper metal to the Cu cation (Cu/Cu^{2+}) (Figure 7a).[15] The electrochemistry of copper complexes in an aqueous medium is sensitive to anions present in the electrolyte solution. When the supporting electrolyte anions are NO_3^- and HPO_4^- ions, Cu^{2+} reduction occurs via a single two-electron transfer process, whereas in Cl^--containing electrolytes, reduction occurs via two one-electron transfer processes, because of stabilization of the Cu^+ species by Cl^-. The Cu^+ ion forms a complex with Cl^- ions ($CuCl_2^-$).[15] The peak potential, which has been altered with respect to scan rate, and the plot of peak current, with respect to the square root of the scan rate, shows linear behavior. This shows that the redox process $(Cu(en)_2^{2+}/Cu)$ is quasi-reversible in nature. On encapsulation in various zeolites (Figure 7b−f), the reduction potential $(Cu(en)_2^{2+}/Cu)$ is altered toward more-negative values and peaks are broadened (see Table 5). The alteration of peak potential toward more-negative values on encapsulation indicates the stabilization of Cu^{2+} oxidation state in zeolite cages. This may be due to axial interaction with the zeolite matrix. The alteration of peak potentials indicates that the metal complex does not have the same geometry as that in

TABLE 6: Optimized Parameters for Neat and Zeolite Cluster-Encapsulated Cu-en Complexes

	Bond Distance (Å)				Bond Angle (deg)			
catalyst	Cu−N_1	Cu−N_2	Cu−N_3	Cu−N_4	∠N_1−Cu−N_2	∠N_3−Cu−N_4	∠N_1−Cu−N_3	∠N_2−Cu−N_4
Cu-en-neat	2.04	2.04	2.04	2.04	85.36	85.36	94.6	94.6
Cu-en-Si_{10}	1.92	1.92	1.92	1.92	83.87	83.87	81.95	81.95
Cu-en-$AlSi_9$	1.92	1.92	1.92	1.92	84.50	84.50	82.01	82.01
Cu-en-Al_2Si_8	1.94	1.94	1.94	1.94	82.80	82.50	82.20	82.20
Cu-en-Si_{12}	1.95	1.95	1.95	1.95	81.74	81.74	84.65	84.65
Cu-en-BSi_{12}	1.89	1.89	1.89	1.89	99.39	99.65	113.37	113.46
Cu-en-$AlSi_{12}$	1.95	1.95	1.95	1.95	81.52	81.52	84.64	84.64
Cu-en-$GaSi_{12}$	1.95	1.95	1.95	1.95	81.51	82.12	84.63	84.63

the neat complex but does undergo distortion inside the zeolite matrix.[51] In the case of NaY and KL zeolites, different electrochemical responses were observed. To ascertain whether different electrochemical responses were due to uncomplexed Cu cations or copper complexes present on the external surface, a cyclic voltammogram was recorded for copper-exchanged NaY, KL, and Naβ zeolites and the physical mixture of copper ethylenediamine and NaY zeolites. The peak potentials for copper-exchanged NaY (Figure 7g), KL (Figure 7h), Naβ (Figure 7i), and the physical mixture of copper ethylenediamine and NaY zeolites (Figure 7j) (the Cu^{2+}/Cu redox process) are totally different from the copper ethylenediamine complex encapsulated in various zeolites. This indicates that a copper ethylenediamine complex is encapsulated inside the zeolite matrix and not present on the external surface. When copper-exchanged zeolites are treated with ethylenediamine, the redox potential Cu^{2+}/Cu shifted toward a more-negative value. This is due to the increase of crystal field stabilization energy as one goes from $Cu(H_2O)_6^{2+}$ to the bis-ethylenediamine copper complex. Because of axial interaction with various zeolites and distortion of metal complexes inside the zeolite matrix, peak potentials are altered in various zeolites. Different electrochemical responses are due to the copper ethylenediamine complex that is present in different positions of zeolites. The charge on the O atom in a given zeolite is not same in all locations of the zeolite (Table 6). The FAU type of zeolite has four type of oxygens with different charges.[52] Similarly, other zeolites have different types of O atoms. The redox potential of a metal complex encapsulated in a given zeolite is dependent on the axial interaction of the metal complex with an O atom of the zeolite matrix and also distortion of the molecule due to steric constraints. The peak broadening is observed after encapsulation of the metal complexes in various zeolites. This is because of axial interaction of metal complex with different types of O atoms in a given zeolite, so that the metal complex exhibits different redox potentials at different places, leading to peak broadening. Because of the partial covalent character of the aluminosilicate crystals, electrons are not localized on the framework atoms; rather, they are partially delocalized.[53] When a metal complex interacts with an active site, it will perturb all the active sites present within the zeolite, so that the complex will have a different interaction energy and altered redox potential at different places in the zeolite.

Charge distribution along the framework due to the partial ionic character of the aluminosilicate crystal generates a strong columbic field inside the cavities, which might activate the metal complex. Field gradients exist because of the zeolite geometry, cages, channels, side packets, and charge distribution.[54] This may alter the energy levels of the metal complex so that metal complexes present at different locations of the zeolite have altered redox potentials.

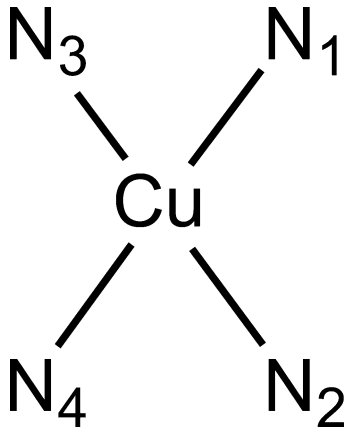

Figure 8. Representation of Cu-en.

4. Theoretical Methods

The redox potential of the metal complex is altered in various zeolites, because of the change in the position of the highest occupied molecular orbital (HOMO) and lowest unoccupied molecular orbital (LUMO) levels of metal complexes. To understand the position of the HOMO and LUMO levels of metal complexes in various zeolites, theoretical calculations were performed using density functional theory (DFT). The optimized N−Cu bond length and N−Cu−N bond angle (represented in Figure 8) for neat and encapsulated complexes are given in Table 6. Table 6 shows that the DFT calculations with the B3LYP functional and LanL2DZ basis set can be used to predict the structure of the neat complex quite reasonably. The neat complex has D_{2h} symmetry. On encapsulation in 10-membered and 12-membered-ring systems, it deviates from square planarity ($D_{2h} \rightarrow C_{2v}$) (Figure 9). The bond length between the metal and the ligand molecule decreases on encapsulation. Quantum chemical calculations have proven that Si−O bonds in zeolites have a clearly covalent character.[55] Valence electrons in zeolites are distributed all over the framework atoms as a partially delocalized electronic cloud. At relatively short distances between the complex molecule and the walls of the zeolite cavities, the electron−electron repulsions will be operative, which will cause the bond length between the Cu ion and the ligand molecule to decrease.

The energy of the HOMO level for the neat complex is located at −15.12 eV, and the main contribution to HOMO comes from the Cu d-orbital (25.78%) and the N p-orbital (58.53%) (see Table 7). A comparison of the energy values of the HOMO and LUMO orbitals of the neat complex with the values obtained inside each cluster is given in Table 7. In the case of encapsulated complexes, the HOMO and LUMO energies of Cu-en are taken from the molecular orbitals that have a marked contribution from the copper ethylenediamine molecule. Encapsulation of the copper ethylenediamine in 10-

TABLE 7: Comparison of HOMO and LUMO Energies of Neat and Zeolite Cluster-Encapsulated Cu-en Complexes and Percentage Contribution of Atomic Orbitals to HOMO and LUMO

		Contribution (%)														
molecular	energy	Si		Al		O		H_{zeo}		Cu		N		C		$H_{complex}$
orbital	(eV)	s	p	s	p	s	p	s	s	p	d	s	p	s	p	s
							Cu-en-neat									
HOMO	−15.21								0.00	0.0.00	25.78	7.62	58.53	3.73	2.93	1.41
LUMO	−8.21								36.48	0.00	0.98	47.44	2.47	1.65	2.75	8.23
							$Cu\text{-en-}Si_{10}$									
HOMO	−12.59	0.00	3.25			0.00	26.21	1.00	0.00	0.00	14.16	6.67	36.8	4.46	3.68	3.77
LUMO	−7.35	1.33	3.86			7.82	2.6 2	0.4	32.13	7.27	0.34	27.35	2.36	4.28	1.11	9.13
							$Cu\text{-en-}AlSi_9$									
HOMO	−13.24	0.00	2.63	0.0	0.04	0.0	6.6	9.52	0.00	0.03	18.73	9.8	43.3	1.7	4.4	3.25
LUMO	−8.19	2.00	5.09	0.1	0.55	10.69	3.54	1.38	22.91	2.22	0.25	31.41	4.39	2.31	0.6	12.56
							$Cu\text{-en-}Al_2Si_8$									
HOMO	−13.99	0.00	0.73	0.00	0.00	0.00	5.46	2.73	0.00	0.00	22.37	11.49	49.99	2.23	0.48	4.52
LUMO	−8.47	0.4	2.7	0.13	0.46	11.95	3.80	0.57	15.16	4.00	0.1	32.22	6.59	9.15	5.93	6.84
							$Cu\text{-en-}Si_{12}$									
HOMO	−12.87	0.0	3.39			0.0	23.29	7.61	0.0	0.00	15.19	7.11	35.86	1.06	3.68	2.81
LUMO	−7.24	0.05	0.49			0.68	1.22	0.07	36.83	6.4	0.03	32.33	3.61	5.25	1.34	11.7

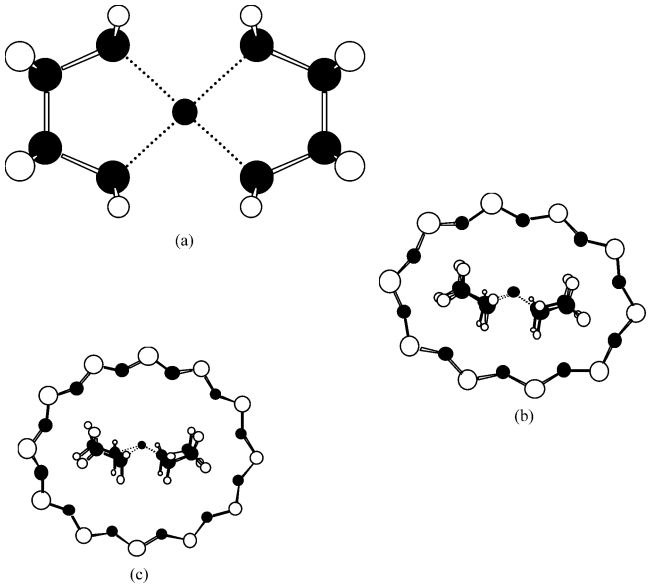

Figure 9. Geometry of (a) Cu-en, (b) $Cu\text{-en-}Si_{10}$, and (c) $Cu\text{-en-}Si_{12}$.

or 12-membered ring systems clearly produces a large increase in the HOMO and LUMO energies (2.3−2.6 eV). The HOMO and LUMO energies are higher in 10-membered-ring systems, compared to those of 12-membered-ring systems. Compared to 12-membered-ring systems, 10-membered-ring systems have a smaller cavity size. This leads to a large amount of stress in 10-membered-ring systems, which increases the HOMO and LUMO energy of the system. The electric field that acts inside the 10-membered-ring systems will be higher, compared to that inside 12-membered-ring systems. This situation leads to an increase of the HOMO and LUMO values of the metal complex in 10-membered-ring systems, compared to those in 12-membered-ring systems.

The type of interaction normally considered when a guest molecule is confined inside the zeolite[56] is due to Coulombic effects, coordination effects, and van der Waals interactions. Coulombic effects are produced by the charge distribution along the framework, because of the partial ionic character of the ionic crystals. This charge distribution generates a strong Coulombic field on the cavities, which might alter the energy level of the metal complexes, as well as influence the chemical behavior of the transition-metal complexes. Coordination effects are produced by Lewis acid−base-type interactions among the transition-metal complexes and certain sites of the framework in the cavity. Weak electron interactions account for the forces of the van der Waals type. One of the effects that have not been examined in the literature is the double-layer effect. The zeolite framework is anionic in nature. When the transition-metal complex enters the zeolite cavity, it forms a double layer in the zeolite cavities. It is known in the literature[57] that the electric field that exists between a double layer is $\sim 10^8$ V/cm. This electric field alters the energy levels and chemical behavior of the transition-metal complexes. Because of these properties, the molecular orbital of the metal complex cannot extend over the entire space but instead is restricted within the dimension of the zeolite cages. The percentage atomic orbital contributions to the HOMO and LUMO energies are given in Table 7. The p-orbital participation of the N atom to the HOMO energy decreases after encapsulation. It shows that overlap between the metal orbital and the ligand orbital decreases after encapsulation.

To rationalize the influence of aluminum content in the position of the HOMO and LUMO levels of the metal complexes, replacement of Si → Al,H was performed in 10-membered-ring systems to form cages with one, two, or three Brønsted sites. The presence of a Brønsted site changes the electrostatic potential generated inside the cage.[19] In a purely siliceous zeolite, a negative electrostatic potential, which is acting inside the cavity, creates a repulsion over the electrons in the complex molecule. This repulsion will increase their energy. If aluminum is introduced, the O → OH change will make the new electrostatic potential less negative, because of proton shielding on the corresponding O atom and the electrostatic repulsion over the electrons is less. This leads to a decrease in the energy level of the metal complexes. When aluminum is introduced in the zeolites, the HOMO and LUMO levels of the metal complexes are stabilized, compared to those in purely siliceous zeolites. To determine if this observation is due to aluminum or not, other trivalent atoms (B, Ga) are substituted in 12-membered-ring systems and Cu-en complex is encapsulated in this modified cluster. The HOMO and LUMO values of the Cu-en complex in this modified cluster are given in Table 8. Both the HOMO and LUMO levels of Cu-en are stabilized in trivalent-ion-substituted systems, compared to those in the

TABLE 8: HOMO and LUMO Values of Cu-en Complex Encapsulated in a Trivalent-Ion-Substituted Twelve-Membered-Ring Cluster

catalyst	HOMO (eV)	LUMO (eV)
Cu-en-Si_{12}	−12.87	−7.24
Cu-en-BSi_{11}	−14.40	−6.71
Cu-en-$AlSi_{11}$	−13.37	−8.08
Cu-en-$GaSi_{11}$	−13.36	−8.06

TABLE 9: Catalytic Activities toward the Oxidation of Dimethyl Sulfide (DMS) by Neat and Encapsulated Cu-en Complexes and Neat and Immobilized Cytochrome-C[a]

catalyst	conversion to dimethyl sulfoxide (mol %)	TON[b]
Cu-en	0	0
Cu-en-NaY	75.1	466
Cu-en-KL	99.3	1383
Cu-en-Naβ	95.0	1050
Cu-en-NaZSM-5	98.8	1597
Cu-en-AlMCM-41	81.3	1313

[a] Reaction conditions for neat and encapsulated Cu-en: mass of catalyst, 100 mg; DMS:H_2O_2 ratio, 1:1; water volume, 5 mL; time, 30 min; and temperature, 303 K. [b] Turn over number, defined as the number of moles of product formed divided by the number of moles of catalyst taken.

purely siliceous zeolite. It shows that aluminum or other trivalent ions are not responsible for stabilization of the HOMO and LUMO levels of the metal complexes.

The generation of a charge-compensating cation reduces the electric field acting inside the cavity that stabilizes the HOMO and LUMO levels of the metal complexes. Because, in zeolites, Al substitution is random, the molecule, which is present in the sodalite cages and the super cages, cannot experience the same electrostatic field. The position of the HOMO and LUMO levels of the metal complexes will be different in different parts of the zeolite, which leads to an altered redox potential of the metal complexes in various positions of the zeolites.

5. Catalytic Activity

The results of the catalytic activity studies performed in the oxidation of dimethyl sulfide (DMS) over the encapsulated and neat Cu-en complexes are presented in Table 9. Liquid-phase oxidation of DMS was performed using neat and encapsulated Cu-en complexes at room temperature. The neat complex is inactive for the oxidation of DMS under these conditions. This may be due to degradation of the metal complexes in the presence of hydrogen peroxide (H_2O_2). On encapsulation in various zeolites, the neat complex exhibits greater activity. The Cu-en complex encapsulated in ZSM-5 exhibits a higher turn over number (TON) value, compared to that of other zeolites. The greater activity of the metal complex in an encapsulated system may be due to alteration of the redox potential of copper ethylenediamine complexes in zeolite cages.

6. Conclusions

The interaction of copper ethylenediamine in the zeolites is dependent on the nature of the zeolite. The maximum wavelength (λ_{max}) of Cu-en was red-shifted or blue-shifted on encapsulation of the metal complexes in various zeolites; the electron paramagnetic resonance (EPR) and bonding parameters of neat and zeolite-encapsulated Cu-en complexes show that the Cu-en complex does not have the same geometry as that in the neat complex. The copper complex may undergo distortion inside the zeolite matrix. The peak potential of the Cu-en complex was altered toward more-negative values on encapsulation in various zeolites. Different electrochemical responses and peak broadening in cyclic voltammetry on encapsulation of metal complexes are due to the metal complexes being located in different locations in the zeolites. Molecular orbital calculations show that the highest occupied molecular orbital (HOMO) and lowest unoccupied molecular orbital (LUMO) level of the Cu-en complex increases when they are encapsulated in zeolite clusters. When trivalent atoms are substituted into the structure, the HOMO and LUMO levels are stabilized. This is due to the presence of charge-compensating cations, which decreases the electric field inside the system. Copper ethylenediamine complexes encapsulated in various zeolites exhibit higher activity, compared to the neat complex. This may be due to alteration of the redox potential of the metal complex inside the zeolites.

Nature is able to perform various electron-transfer reactions efficiently because it can manipulate the redox potential of metal complexes by encapsulating them in various protein mantles. This present study shows that, by changing the redox potential of a given metal complex, which is inactive for a particular reaction under a given set of conditions, one can make it an active catalyst. This study provides a vital clue for generating efficient biomimetic systems in the future.

References and Notes

(1) Velde, F. V. D.; Arends, I. W. C. E.; Sheldon, R. A. *J. Inorg. Biochem.* **2000**, *80*, 81.
(2) Varkey, P.; Jacob, S.; Chandra, R. *Indian J. Chem. A* **1998**, *37A*, 407.
(3) Sheldon, R. A.; Arends, I. W. C. E.; Lempers, H. E. B. *Catal. Today* **1998**, *41*, 387.
(4) Clark, W. M. *Oxidation and Reduction Potential of Organic Systems*; The Williams and Wilkins Company: Baltimore, MD, 1960; p 451.
(5) Viswanathan, B. *J. Energy, Heat Mass Transfer* **1996**, *18*, 281.
(6) Alvaro, M.; Carbonell, E.; Domenech, A.; Fornes, V.; Garcia, H.; Narayana, M. *Chem. Phys. Phys. Chem.* **2003**, *4*, 483.
(7) Fan, B.; Fan, W.; Li, R. *J. Mol. Catal. A: Chem.* **2003**, *201*, 137.
(8) Jacob, C. R.; Varkey, S. P.; Ratnasamy, P. *Appl. Catal., A* **1999**, *182*, 91.
(9) Jacob, C. R.; Varkey, S. P.; Ratnasamy, P. *Microporous Mesoporous Mater.* **1998**, *22*, 465.
(10) Ray, S.; Vasudevan, S. *Inorg. Chem.* **2003**, *42*, 1711.
(11) Flentge, D. R.; Lunsford, J. H.; Jacobs, P. A.; Uytterhoeven, V. *J. Phys. Chem.* **1975**, *79*, 354.
(12) Peigneur, P.; Lunsford, J. H.; Wilde, W. D.; Schoonheydt, R. A. *J. Phys. Chem.* **1977**, *81*, 1179.
(13) Bohlmann, W.; Michel, A. P. D. *Colloid. Surf. A* **1999**, *158*, 235.
(14) Rolison, D. R.; Bessel, C. A.; Baker, M. D.; Senaratne, C. Z. J. *J. Phys. Chem.* **1996**, *100*, 8610.
(15) Senaratne, C.; Zhang, J.; Baker, M. D.; Bessel, C. A.; Rolison, D. R. *J. Phys. Chem.* **1996**, *100*, 5849.
(16) Bessel, C. A.; Rolison, R. *Stud. Surf. Sci. Catal.* **1995**, *98*, 114.
(17) Briot, E.; Bedioui, F.; Balkus, K. J., Jr. *J. Electroanal. Chem.* **1998**, *454*, 83−89.
(18) Gaillon, L.; Sajot, N.; Bedioui, F.; Devynck, J.; Balkus, K. J., Jr. *J. Electroanal. Chem.* **1993**, *345*, 157.
(19) Vogel, A. I. *Quantitative Inorganic Analysis*; Longmans, Green, and Co.: New York, 1953; p 433.
(20) Corma, A.; Garcia, H.; Sastre, G.; Viruela, P. M. *J. Phys. Chem.* **1997**, *101*, 4575.
(21) Powell, D. B.; Sheppard, N. *J. Chem. Soc.* **1959**, 791−796.
(22) Armengol, I.; Corma, A.; Fornes, V.; Garcia, H.; Primo, J. *Appl. Catal., A* **1999**, *181*, 305.
(23) Seelan, S.; Sinha, A. K.; Srinivas, D.; Sivasankar, S. *J. Mol. Catal. A: Chem.* **2000**, *157*, 163.
(24) Gerrits, P. P. K.; Verberckmoes, A.; Schoonheydt, R.; Ichikawa, M.; Jacobs, P. A. *Microporous Mesoporous Mater.* **1998**, *21*, 475.
(25) Bennur, T. H.; Srinivas, D.; Ratnaswamy, P. *Microporous Mesoporous Mater.* **2001**, *48*, 111.
(26) Lu, G.; Guczi, L. *Stud. Surf. Sci. Catal.* **1994**, *83*, 347.
(27) Guczi, L.; Lu, G.; Zsoldos, Z.; Koppany, Z. *Stud. Surf. Sci. Catal.* **1994**, *84*, 949.
(28) Lewis, W. B.; Alei, M., Jr.; Morgan, L. O. *J. Chem. Phys.* **1966**, *45*, 4003.
(29) Wasson, J. R.; Trapp, C. *J. Phys. Chem.* **1969**, *73*, 3763.
(30) Gersmann, H. R.; Swalen, J. D. *J. Chem. Phys.* **1962**, *36*, 3221.

(31) Jacob, C. R.; Varkey, S. P.; Ratnasamy, P. *Appl. Catal., A* **1998**, *168*, 354.
(32) Chavan, S.; Srinivas, D.; Ratnasamy, P. *J. Catal*. **2000**, *192*, 286.
(33) Tomlinson, A. A. G.; Hathaway, B. J. *J. Chem. Soc. A* **1968**, 1685.
(34) Yokoi, H.; Addison, A. W. *Inorg. Chem*. **1977**, *16*, 1341.
(35) Holm, R. H.; Chakravorthy, A.; Theriot, L. J. *Inorg. Chem*. **1966**, *5*, 625.
(36) Sinn, E.; Harris, C. M. *Coord. Chem. Rev.* **1969**, *4*, 391.
(37) Billing, D. E.; Dudley, R.; Hathaway, B. J.; Nicholls, P.; Procter, I. M. *J. Chem. Soc. A* **1969**, 312.
(38) Mopourgo, L.; Williams, R. J. P. *J. Chem. Soc. A* **1966**, 73.
(39) Maki, A. H.; McGarvey, B. R. *J. Chem. Phys.* **1958**, *29*, 31.
(40) Neimann, R.; Kivelson, D. *J. Chem. Phys.* **1961**, *35*, 149.
(41) Procter, I. M.; Hathaway, B. J.; Nicholls, P. *J. Chem. Soc. A* **1968**, 1678.
(42) Herman, R. G.; Flentge, D. R. *J. Phys. Chem.* **1978**, *82*, 720.
(43) Herman, R. G. *J. Catal.* **1979**, *34*, 119.
(44) Dedecek, J.; Sobalik, Z.; Tvaruzkova, Z.; Kaucky, D.; Witcherlova, B. *J. Phys. Chem.* **1995**, *99*, 16327.
(45) Carl, P. J.; Larson, S. C. *J. Phys. Chem. B* **2000**, *104*, 6568−6575.
(46) Carl, P. J.; Baccam, S. L.; Larson, S. C. *J. Phys. Chem. B* **2000**, *104*, 8848.
(47) Yu, J. S.; Kevan, L. *J. Phys. Chem.* **1994**, *98*, 12436.
(48) Yu, J. S.; Kevan, L. *J. Phys. Chem.* **1993**, *97*, 11047.
(49) Oliver, C.; Selli, E.; Ponti, A.; Correale, L.; Solinas, V.; Rombi, L.; Monaci, R.; Forni, L. *J. Chem. Soc., Faraday Trans.* **1997**, *93*, 2603.
(50) Xu, J.; Yu, J. S.; Lee, S. J.; Kim, B. Y.; Kevan, L. *J. Phys. Chem. B* **2000**, *104*, 1307.
(51) Addison, A. W. *Inorg. Chim. Acta* **1989**, *162*, 217.
(52) Vangenechten, K. A.; Mortier, W. J. *Zeolites* **1988**, *8*, 273.
(53) Utterhoeven, L.; Dompass, D.; Mortier, W. J. *J. Chem. Soc., Faraday Trans.* **1992**, *88*, 2753.
(54) Janssens, G. O. A.; Baekelandt, B. G.; Toufar, H.; Mortier, W. J.; Schoonheydt, R. A. *J. Phys. Chem.* **1995**, *99*, 3251.
(55) Sauer, J. *Chem. Rev.* **1989**, *89*, 199.
(56) Zicovich-Wilson, C. M.; Corma, A.; Viruela, P. *J. Phys. Chem.* **1994**, *98*, 10863.
(57) Bard, A. J.; Faulkner, L. R. *Electrochemical Methods. Fundamentals and Applications*, Second ed.; Wiley: New York, 2001; p 115.